PAPER

Evaluating the solid electrolyte interphase formed on silicon electrodes: a comparison of *ex situ* X-ray photoelectron spectroscopy and *in situ* neutron reflectometry†

T. M. Fears,‡*[a] M. Doucet,*[b] J. F. Browning,*[c] J. K. S. Baldwin,[d] J. G. Winiarz,[a] H. Kaiser,[e] H. Taub,[f] R. L. Sacci[g] and G. M. Veith*[g]

This work details the *in situ* characterization of the interface between a silicon electrode and an electrolyte using a linear fluorinated solvent molecule, 0.1 M lithium bis(trifluoromethanesulfonyl)imide (LiTFSI) in deuterated dimethyl perfluoroglutarate (d_6-PF5M$_2$) (1.87×10^{-2} mS cm^{-1}). The solid electrolyte interphase (SEI) composition and thickness determined *via in situ* neutron reflectometry (NR) and *ex situ* X-ray photoelectron spectroscopy (XPS) were compared. The data show that SEI expansion and contraction (breathing) during electrochemical cycling were observed *via* both techniques; however, *ex situ* XPS suggests that the SEI thickness increases during Si lithiation and decreases during delithiation, while *in situ* NR suggests the opposite. The most likely cause of this discrepancy is the selective removal of SEI components (top 20 nm of the SEI) during the electrode rinse process, which is required to remove the electrolyte residue prior to *ex situ* analysis, demonstrating the necessity of performing SEI characterization *in situ*.

1. Introduction

The solid electrolyte interphase (SEI) is a protective solid barrier that forms on the surface of a lithium-ion battery operating outside the stability range of an electrolyte; particularly at the anode where during a lithiation reaction the Li metal reduces the liquid electrolyte forming a solid mixture of inorganic and organic components.[1–3] The SEI is an integral, yet under-characterized component of Li-ion batteries. If the reaction does not proceed properly, the electrolyte will continue to react causing a reduction in cell capacity and reduce ion transport

to the battery electrode. In addition, a poor interfacial layer will result in electrical contact, shorting, within the cell leading to an increased risk in fire or other catastrophic events. A good barrier layer prevents additional electrolyte decomposition. Furthermore, the SEI prevents the exfoliation of the anode material during cycling.[1–3] To optimize battery performance and predict better electrolyte chemistries for more ideal SEI formation reactions, a detailed study of the relationship between SEI composition and properties is required. This is particularly important for more advanced, higher capacity anodes like silicon (>3000 mA h g^{-1} theoretical capacity *versus* ~ 330 mA h g^{-1} for conventional graphite) which provide an opportunity to obtain higher gravimetric capacities but have large volume changes which pulverize the material exposing new surfaces which require the formation of additional SEI components.[3]

The SEI is typically a 5–50 nm layer on 1–100 μm particles, so the SEI is only a low compositional fraction and must be analyzed using surface-sensitive techniques or grown on high-surface-area materials to obtain sufficient signal intensity.[1,3–9] The most common methods of characterizing SEIs, *e.g.* X-ray photoelectron spectroscopy (XPS), infrared absorption spectroscopy (IR), and nuclear magnetic resonance spectroscopy (NMR), involve disassembling cycled Li-ion cells and often rinsing the electrode of interest to remove an excess of electrolyte before analysis.[1,3,9,10] These preparation steps potentially remove soluble

[a] *Department of Chemistry, Missouri University of Science and Technology, 400 W. 11th St., Rolla, MO 65409, USA. E-mail: fears1@llnl.gov*

[b] *Neutron Data Analysis and Visualization Division, Oak Ridge National Laboratory, 1 Bethel Valley Rd., Oak Ridge, TN 37831, USA. E-mail: doucetm@ornl.gov*

[c] *Chemical and Engineering Materials Division, Oak Ridge National Laboratory, 1 Bethel Valley Rd., Oak Ridge, TN 37831, USA. E-mail: browningjf@ornl.gov*

[d] *Materials Science and Technology Division, Los Alamos National Laboratory, Los Alamos, NM 87545, USA*

[e] *University of Missouri Research Reactor, University of Missouri, 1513 Research Park Dr., Columbia, MO 65211, USA*

[f] *Department of Physics and Astronomy, University of Missouri, Columbia, MO 65211, USA*

[g] *Materials Science and Technology Division, Oak Ridge National Laboratory, 1 Bethel Valley Rd., Oak Ridge, TN 37831, USA. E-mail: veithgm@ornl.gov*

† Electronic supplementary information (ESI) available. See DOI: 10.1039/c6cp00978f

‡ U.S. Department of Energy, Office of Science Graduate Student Research Program Fellow, Oak Ridge National Laboratory.

This journal is © the Owner Societies 2016

Phys. Chem. Chem. Phys., 2016, **18**, 13927–13940 | **13927**

SEI components and expose the electrode to environmental contaminants.[10,11] *In situ* characterization avoids such effects and has the potential to monitor transient and dynamic interactions.[10–20]

For this study, neutron reflectometry (NR) was chosen to investigate the SEI formed on a Si thin film, as it possesses several advantages over other methods. X-ray and neutron reflectometry are interface-sensitive techniques,[1,21–26] unlike diffraction or nuclear magnetic resonance, and interrogate a macroscopic sample size, unlike electron microscopy. Neutrons are deeply penetrating and sensitive to light elements (H and Li),[12,16,18,25–28] unlike X-rays, making NR particularly suited for the characterization of SEIs and electrodes in Li-ion batteries.[12,16,18,25–28] A specialized cell has been developed at the Oak Ridge National Laboratory for use on a Liquids Reflectometer (Spallation Neutron Source, Beam Line 4B) for performing NR on thin films during electrochemical cycling. Analysis of these data provides information on the thickness, roughness, and composition of various layers within the battery.[25] Prior work has revealed the formation of a 17 to 25 nm SEI layer in ethylene carbonate/dimethyl carbonate (EC/DMC) electrolytes whose composition and thickness change with cycling.[26] Other *in situ* NR studies have shown the formation of a 5.5 nm reaction layer on TiO_2,[29] a 20 nm thick layer that forms at the electrode/electrolyte interface on $LiFePO_4$,[30] and a 7 nm electrochemical SEI layer that is formed only upon delithiation, though the extent of lithiation was not clear.[21] More recently, we demonstrated the formation of a 3.3 nm Li-rich layer at open circuit voltage on the high voltage cathode $LiMn_{1.5}Ni_{0.5}O_4$ which changed with charging to become a F-rich layer with a similar thickness[24] while others have focused on electrolyte decomposition over Cu metal as a function of potential.[22]

One commonality of all these prior studies is the use of carbonate based solvents given their importance to battery technology; however the neutron scattering properties of these carbonate molecules are not optimal for *in situ* neutron studies. For example, hydrogen (^1H) possesses a large, incoherent neutron scattering cross-section (80.26 barns (b)), so the presence of a hydrogenous material in an electrochemical cell can contribute significantly to the background signal in elastic neutron scattering techniques like NR or powder diffraction. In addition, for these NR studies one wants an electrolyte with a high scattering length density (SLD) to provide maximal contrast; when possible, the isotopic substitution of deuterium (^2H) for naturally abundant H (99.99% ^1H) is carried out to increase the SLD, as ^2H has a positive scattering length (6.67 fm) and a small incoherent cross-section (2.05 b) while ^1H has a negative scattering length (-3.74 fm) and a large incoherent scattering cross-section. Commercially available deuterated carbonates are also only of moderate (99%) purity,[26] leading to electrochemical side reactions which can result in an unintentional modification of electrodes and SEI chemistry. An alternative approach to obtaining an appropriate electrolyte involves the use of fluorinated solvents which have high SLDs and low incoherent scattering cross-sections due to the F atoms (5.65 fm, 0.0008 b) and can be prepared at high ($>99.9\%$) purity.[31] In addition, fluorinated solvents and additives have a number of other advantageous properties for Li-ion battery

electrolytes: high oxidation potential, low flammability, and attractive SEI characteristics.[1,4,8,32–34] The use in this work of a simple fluorinated electrolyte serves to aid in understanding the role of fluorinated additives and solvents in the formation and final properties of SEIs formed in next-generation electrolytes which utilize such components.

To investigate potential fluorinated electrolyte solvents, d_6-dimethyl perfluoroglutarate was synthesized with high ($\geq 99.9\%$) purity and used as a low-scattering electrolyte solvent for *in situ* NR. The electrochemical properties of a series of perfluorocarboxylate ester based electrolytes have been previously reported along with an in-depth *ex situ* chemical characterization of the SEI formed on Si electrodes *via ex situ* XPS.[31] This study further investigates the SEI formed by dimethyl perfluoroglutarate using *in situ* NR for comparison with *ex situ* XPS. The relationship between the state-of-charge (SOC) of the Si electrode and the SEI composition and thickness differs when analyzed *via ex situ* XPS and *in situ* NR, demonstrating the importance of *in situ* characterization.

2. Materials and methods

All reagents were used as received unless otherwise noted. Those used in Li-ion battery cells were stored in a dry Ar-filled glovebox (<5.0 ppm O_2, <100 ppb H_2O) prior to cell fabrication.

2.1 Perfluorocarboxylic acid esterification

Dimethyl perfluoroglutarate ($PF5M_2$) was synthesized as reported previously *via* the esterification of perfluoroglutaric acid (Exfluor, 98%) using methanol (MeOH) (Sigma-Aldrich, $\geq 99.8\%$) or deuterated methanol (99.8% D, Fisher Scientific) to produce protiated and deuterated solvents as necessary. As-distilled esters were dried by storing over 3A molecular sieves (Alfa Aesar) in an Ar-filled glovebox for two weeks.

^1H (400 MHz) nuclear magnetic resonance (NMR) and ^{13}C (100 MHz) NMR with inverse-gated ^1H decoupling were performed on a Varian Unity Inova and used to verify ester synthesis. Purity was determined using the integral of the CH_3 peak in the ^1H spectrum of the ester and trace MeOH, the only detectable impurity (ester: 4.0 ppm in ^1H and 54.2 ppm in ^{13}C *vs.* tetramethylsilane (TMS); MeOH: 3.3 ppm and 3.6 ppm in ^1H and 48.6 ppm in ^{13}C *vs.* TMS).

2.2 Fabrication of an electrochemical cell for *in situ* neutron reflectometry

The thin-film working electrode was deposited by DC magnetron sputtering and evaporation from commercially available targets, Cu (99.99% – Kurt J. Lesker) and Si (99.99% – Kurt J. Lesker), in an in-house sputtering system. Base pressures were below 5×10^{-8} Torr before Cu sputter deposition and the target to substrate distances were 5 cm. Rates were measured using a quartz crystal microbalance. The Cu films were deposited by DC sputtering at an applied power of 300 W, at 3 mTorr Ar (99.9995%, Air Liquide) for 2 min. The amorphous Si films were deposited by thermal evaporation in a chamber with a base
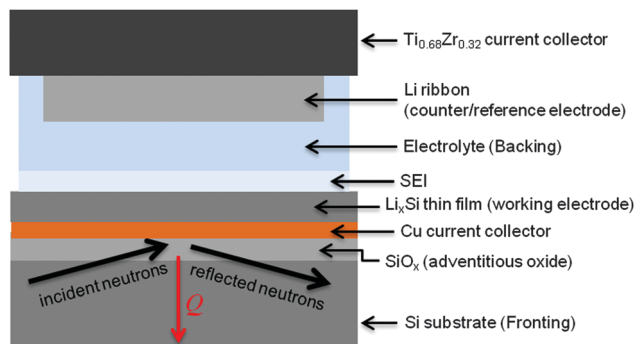
13928 | *Phys. Chem. Chem. Phys.*, 2016, **18**, 13927–13940

This journal is © the Owner Societies 2016

Fig. 1 Experimental geometry for collecting NR data.

pressure less than 5×10^{-9} Torr. The samples were not exposed to air between depositions. 50 mm-diameter, 10 mm-thick single-crystal Si substrates were obtained from the Institute of Electronic Materials Technology, Warszawa, Poland.

$Ti_{0.68}Zr_{0.32}$ alloy (subsequently referred to as TiZr) was selected as the Li current collector for two reasons: (1) TiZr is a null (SLD = 0, incoherent) scatterer of neutrons, eliminating the possibility of interfering diffraction peaks in the NR pattern and (2) TiZr does not react chemically or electrochemically with Li. A machined 50 mm-diameter, 1 cm-thick TiZr substrate was cleaned successively in water and isopropanol sonication baths and dried at 120 °C for 2 days. The Li counter electrode (2.9 cm diameter) was prepared using 3/4″-wide Li-foil (Alfa Aesar), which was scraped clean and pressed onto the TiZr substrate in a dry Ar-filled glovebox.

Wires were attached to the Si and TiZr plates (prior to Li deposition) using silver epoxy (Illinois Tool Works) which were allowed to dry overnight. Silver epoxy was placed on the edge of the Si wafer to come into contact with Cu, which was spilled around the wafer during deposition. The epoxy never came into contact with the electrolyte. Electrodes and 0.1 M LiTFSI in the d_6-PF5M$_2$ electrolyte were sealed under dry Ar and transferred to a He-filled glovebox (H_2O < 1 ppm; O_2 < 7 ppm) located at the beam line for on-site cell assembly.

The *in situ* electrochemical cell for NR was assembled using a specially developed apparatus as previously reported.[24–26] The electrodes were separated by a 48 mm diameter Teflon-coated Viton O-ring with a 0.8 mm cross-sectional diameter. The total cell volume was ~2.5 mL, depending on the amount of Li on the TiZr. This volume was filled with the electrolyte using ports in the TiZr current collector, which were subsequently sealed with Teflon plugs. A diagram of the assembled cell and NR geometry is shown in Fig. 1.

2.3 *In situ* electrochemistry and neutron reflectometry

Electrochemistry was controlled using a Biologic VSP potentiostat. Due to the high resistance of the *in situ* cell, galvanostatic cycling was not possible, so the cell was cycled using a hybrid galvanostatic-potentiostatic protocol. Electrodes were driven galvanostatically (375 μA) to the desired potential and held potentiostatically for 30 min. The cell was then allowed to equilibrate in the open-circuit state for 30 min prior to NR data

collection. Voltages were reported with respect to the Li metal counter electrode (Li/Li$^+$).

NR measurements were carried out on a Liquids Reflecto-meter (LR, Beam Line 4B) at the Spallation Neutron Source (SNS) at Oak Ridge National Laboratory. The LR is a horizontal-geometry instrument which uses the time-of-flight technique with an effective single bandwidth of 3.5 Å at an accelerator pulse frequency of 60 Hz. NR measurements on the assembled cell were carried out in the inverted geometry, using the Si substrate as the incident medium, in order to eliminate anomalous scattering from any potential bubble formation at the top surface of the cell. NR was performed on the as-fabricated electrode in the traditional geometry, with air as the incident medium, in order to determine the initial multilayer parameters prior to any chemical interaction with the electrolyte. For these measurements, neutrons of wavelengths 2.5 Å to 17 Å together with four angles of incidence, θ = 0.60°, 0.69°, 1.37°, and 2.71°, provided a wave vector transfer (Q) range extending from 0.008 Å^{-1} to 0.22 Å^{-1}. An incident beam slit was adjusted for each angle in order to maintain a constant footprint on the sample.

Reflected neutrons are collected in a two-dimensional position sensitive detector. These data are processed using the Mantid data analysis framework to obtain the reflectivity profile.[35] The background intensity from incoherent and inelastic scattering is determined from the off-specular intensity and subtracted from the specular intensity (ESI,† Fig. S1). The final reflectivity is obtained by absolutely normalizing the resulting intensity using attenuation parameters experimentally determined from an uncoated single-crystal Si substrate.

2.4 Fitting of neutron reflectometry data

Modeling of the neutron reflectivity data was done using the Motofit program.[27] Due to the difficulty in background subtraction at low signal intensity, fitting was only performed up to Q = 0.1 Å^{-1}. The details of the analysis, including the estimation of the uncertainties, can be found in a previous study.[26] Model constraints were added to analysis described in the reference stated above using the well-defined relationship between the Li$_x$Si alloy stoichiometry and the unit cell volume,[36]

$$\frac{V}{V_0} - 1 + 0.775x \tag{1}$$

where V and V_0 are Li$_x$Si alloy and elemental silicon volumes, respectively, and x is the Li/Si ratio. Assuming one-dimensional swelling typical of thin films, the thickness and SLD of the Li$_x$Si layer were constrained to a single fitting parameter. Fitting of the NR profile provides a thickness and SLD (β) for each layer. The SLD is indicative of the atomic composition of the layer and can be calculated using the following equation:

$$\beta = \sum_i N_{d,i} b_i = N_d \sum_i \chi_i b_i \tag{2}$$

where $N_{d,i}$ is the number density of nucleus i, b_i is the neutron scattering length of nucleus i, N_d is the average atomic number density of the layer, and χ_i is the molar fraction of nucleus i.

This journal is © the Owner Societies 2016

Phys. Chem. Chem. Phys., 2016, **18**, 13927–13940 | **13929**

2.5 *Ex situ* characterization

Si thin-film electrodes were prepared *via* radio-frequency (RF) magnetron sputtering using an undoped Si target under Ar at 7.5 mTorr and 90 W RF power. The deposition rate was determined to be 8 nm min^{-1} using a quartz crystal microbalance (Inficon). Si was deposited for 10 min onto a rough electrochemical-grade Cu foil (Oak-Mitsui). The Si films were then cut into either 13 mm- or 8 mm-diameter electrodes as necessary.

The effect of cycling on electrolyte composition was investigated *via ex situ* NMR. Cycled electrolytes were prepared by galvanostatically (10 μA) discharging electrolytes for 18 h in a two-electrode Swagelok-type cell with an 8 mm Si thin-film working electrode and a Li counter electrode and ∼1 mL protiated or deuterated electrolytes. Two layers of a 0.14 mm-thick PEEK mesh (McMaster Carr) were used as a separator in order to ensure a large electrolyte volume for analysis. Swagelok cells were disassembled in a dry Ar glovebox and ∼0.75 mL of each cycled and uncycled electrolyte was transferred to a 5 mm NMR tube. The tubes were then sealed with a polypropylene cap followed by placing a thin bead of epoxy (Loctite Hysol 1C) on the lip of the polypropylene cap for air-tightness before removing from the glovebox. ^{1}H (400 MHz), ^{13}C (101 MHz) with inverse-gated ^{1}H decoupling, ^{19}F (376 MHz), and ^{7}Li (155 MHz) NMR were carried out on a Bruker Avance III spectrometer. ^{1}H spectra were referenced to the most intense impurity signal (1.35 ppm *vs.* TMS). ^{13}C and ^{19}F spectra were referenced to the most intense CF$_2$ peak (109.43 ppm *vs.* TMS and −119.60 ppm *vs.* CFCl$_3$, respectively). These secondary references were chosen in order to avoid isotopically induced shifts from deuteration on the CH$_3$ signal (0.04 ppm in ^{1}H and 0.70 ppm in ^{13}C). Due to the absence of an accurate (<0.01 ppm) secondary standard, ^{7}Li peaks were set to 0 ppm and are only used to demonstrate changes in peak width and intensity with cycling.

The atomic composition of the SEI formed on Si thin-film electrodes was characterized as a function of SOC *via ex situ* XPS. CR2023 stainless steel coin cells (Pred Materials) were prepared using Li ribbons, porous polypropylene separators (Treopore) wetted with an electrolyte, and 13 mm Si thin-film electrodes. Coin cells were galvanostatically cycled at 10 μA, corresponding to an approximate cycling rate of C/10 (fully discharged in 10 h), on a Maccor 4000 battery cycler and stopped at specific potentials related to observed electrochemical reactions. Cycled coin cells were then transferred into a dry Ar-filled glovebox for decrimping. Electrodes were rinsed with 2 mL of DMC (Aldrich, 99.9%) to remove an excess of electrolyte, dried under vacuum, and sectioned for *ex situ* analysis of insoluble SEI components. Electrodes were transferred from the glovebox to the XPS sample stage under vacuum in a specially developed transfer chamber to prevent decomposition upon exposure to air. XPS data were collected on a PHI 3056 with an Al anode source operating at 15 kV and 350 mA. High-resolution spectra were collected using a pass energy of 5.85 eV with 0.05 eV steps. Peak fitting and quantitative elemental analysis were performed using the PHI Multipak analysis suite and standard sensitivity factors. Binding energies were referenced to the C 1s C–H peak (284.8 eV).

3. Results and discussion

This work investigates the SEI formation over an amorphous silicon electrode material. In a "full-cell" configuration, balanced cathode-anode capacities, the silicon would be the anode with a potential of about 0.2 V (*vs.* Li/Li$^+$). In this study the cell is run in a "half-cell" configuration where there is an excess of Li species from a pure Li foil and the reported potential is relative to the standard Li/Li$^+$ potential (∼3.05 V *vs.* SHE).

^{13}C and ^{1}H NMR revealed that both protiated and deuterated esters were of much higher purity (>99.9 mole%) than commercially available deuterated carbonates typically used for *in situ* neutron scattering studies;[26] however these solvents had little solubility for most Li salts. The exception was LiTFSI, which is able to dissolve up to 0.1 M, resulting in an ionic conductivity of 1.87×10^{-2} mS cm^{-1}, far too low for use in a standard composite battery formulation but sufficient for experimental investigation. Although, given the reduction potential of the electrolyte it may be a good additive for other electrolyte formulations and can also serve as a model to provide insight into the chemistry of more conventional fluorinated electrolytes. Analysis of off-specular scattering and diffuse scattering profiles (ESI,† Fig. S1 and S2) demonstrates that perfluorocarboxylates have small scattering cross-sections, suggesting that these solvents may be useful for developing *in situ* neutron scattering studies.

3.1 *In situ* interface characterization using neutron reflectometry

Previous results enabled us to identify regions of interest for *in situ* NR studies.[31] The differential capacity (dQ_C/dV) curve for the first cycle of a Si thin-film coin cell cycled galvanostatically at 10 μA is shown in Fig. 2. The major electrochemical reactions that take place during the first lithiation of Si thin-film electrodes with a 0.1 M LiTFSI in the PF5M$_2$ electrolyte are as follows: SEI formation, ∼1.0 V (Fig. 2, green); adventitious oxide lithiation, 0.48 V (orange); irreversible Si lithiation feature, 0.26 V (blue); first lithiation step, 0.21 V (red); second lithiation step, <0.07 V (red); and delithiation, 0.40 V and 0.54 V (red).[31] Furthermore, additional coin cells were cycled to 0.6 V, 0.4 V, 0.2 V, 0.07 V, and 2.5 V (Fig. 2, black arrows) for *ex situ* XPS investigations to support the NR investigation of the SEI chemistry. A detailed analysis of the chemical composition and evolution of the SEI as determined *via ex situ* XPS is discussed elsewhere.[31]

Fig. 3 shows the voltage and current profiles for the electrode used in the *in situ* NR cell as a function of time. The NR data were collected during the rest steps for the voltage and current collection. While the cycling of battery materials is typically performed galvanostatically (constant current), the high resistance of the electrode used in the NR cell (>1 kΩ) resulted in a large *iR* loss which made stopping at predetermined states of charge difficult. For this reason, a hybrid galvanostatic-potentiostatic (constant voltage) protocol was utilized. Holding the electrode at a predetermined potential allowed the current to decay thereby mitigating the *iR* loss and allowing for comparison
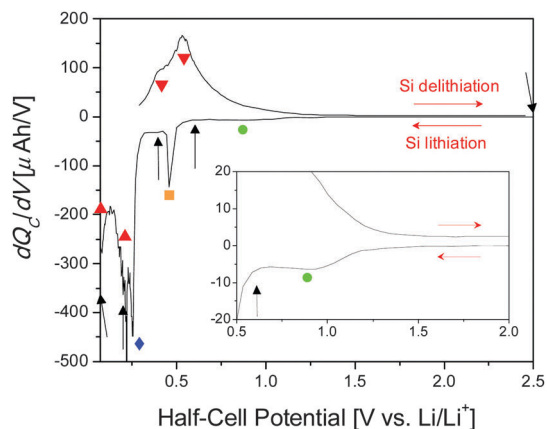
13930 | *Phys. Chem. Chem. Phys.*, 2016, **18**, 13927–13940

This journal is © the Owner Societies 2016

Fig. 2 Differential capacity curve for the first cycle of a Si thin-film half-cell used for *ex situ* analysis. Black arrows mark stopping potentials for *ex situ* XPS. Shapes mark identified electrochemical reactions: SEI formation (green ●), SiO$_2$ lithiation (orange ■), irreversible lithiation (blue ◆), Si lithiation (red ▲), and Si delithiation (red ▼).

with a traditional cell with a lower resistance, *i.e.* a coin cell. After the potentiostatic hold, an additional relaxation step was performed at open circuit to allow for cell equilibration, *e.g.* Li redistribution, to prevent compositional changes from occurring during NR data collection. Even though the cell was allowed to

relax at open circuit for 30 min prior to the collection of NR data, continued potential relaxation during NR data collection is apparent; however, this relaxation is relatively small, implying that any additional changes in the electrode and SEI are minimal and acceptable. Furthermore, as our goal was to characterize the SEI structure small changes in Li–Si chemistry will not influence the SEI chemistry significantly.

3.2 Neutron reflectometry

The *in situ* electrode used in this study was initially measured in air in order to determine the thickness of the Si working electrode, Cu current collector, and adventitious oxide layers before any chemical or electrochemical reactions took place. It was determined that the Si electrode and copper current collectors were 48.3 and 7.4 nm thick, respectively, and that there was a 2.3 nm SiO$_2$ layer between the single-crystal Si substrate and the Cu current collector (ESI,† Table S1). Adding a SiO$_2$ layer on the surface of the Si electrode in the model did not improve the fit quality, so it is assumed that any adventitious oxide on the surface of the electrode is negligible or contrast matched to the electrolyte. This is confirmed by the XPS studies discussed below. Neutron reflectivity curves obtained for the electrode at different cell potentials and the corresponding fits to the data fits are shown in Fig. 4A–I. From these
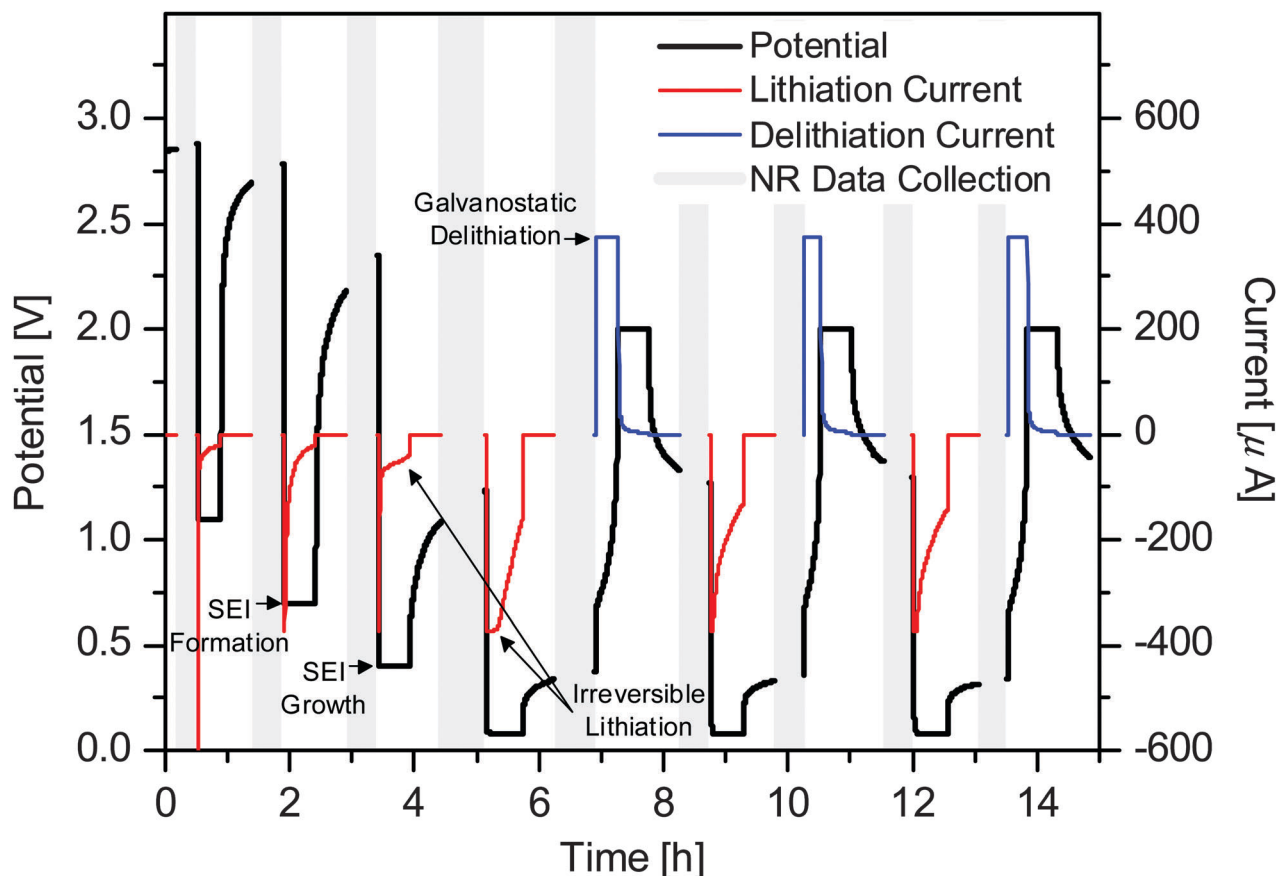

Fig. 3 Electrochemical data for *in situ* NR cells. NR data were collected during the gaps (grey). The voltage profile is shown in black while the current profile is shown in red (lithiation) and blue (delithiation).

data one can see no change in the OCV and 1.1 V data indicating no change in the Si electrode stoichiometry and no clear formation of a condensed surface layer or SEI reaction product. Furthermore, analysis of the in-air (not shown) and OCV NR profiles indicates that no changes occur to the electrode upon exposure to the electrolyte.

However, there are subtle but clear differences in the reflectometry profile at high Q upon reaching 0.7 V, where we see evidence for SEI formation in the electrochemical data (Fig. 2). Fitting this profile revealed a minor expansion of the Si layer (48.3 to 48.9 nm) due to slight lithiation and the formation of a 14.4 nm surface reaction layer attributed to the SEI. Fig. 5 shows a representation of SLD as a function of distance from the Cu/Si interface determined from the fits to the NR data. The SEI layer is indicated by the arrows at the inflection point in the curve. This layer does not appear as a distinct well defined heterostructure. Instead it appears to be a diffuse layer between the

silicon anode and the bulk electrolyte. Removing this layer from the structural models prevents obtaining good fits of the data, and the poor sensitivity to the layer chemistry is reflected in the errors. The large errors are due to the large roughness parameters, which prevent us from seeing a well-defined layer in the SLD profile. It should be noted that a roughness parameter in the model does not allow us to differentiate between a surface roughness and compositional gradients. Fig. 5 and Table 1 show that the SEI has a refined SLD of 4.5 which is lower than the SLD of the electrolyte (4.8×10^{-6} Å^{-2}). This lower SLD has to be due to the formation of a phase with slightly higher Li content than the bulk electrolyte or a film made from the electrolyte but with a lower density than the electrolyte. Given that a significant decrease in density with solid formation is unlikely and additional evidence of Li in the SEI layer (discussed below), this reduction in SLD is attributed to an increase in the Li content of the SEI. Upon continued lithiation (0.4 V) we see a further loss in
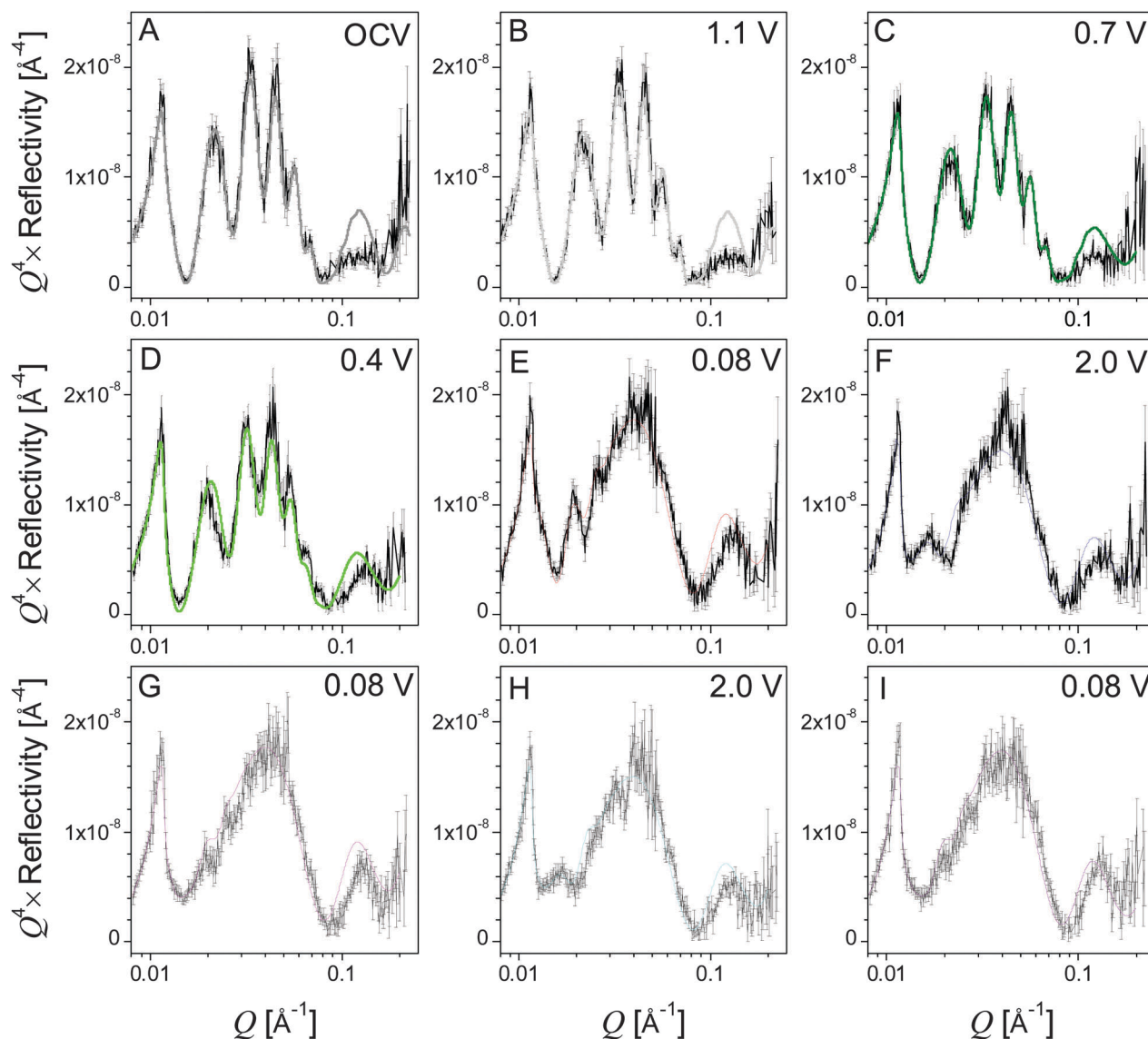

Fig. 4 NR data (black points) and fits (colored lines) in order of collection (A–I).

13932 | *Phys. Chem. Chem. Phys.*, 2016, **18**, 13927–13940
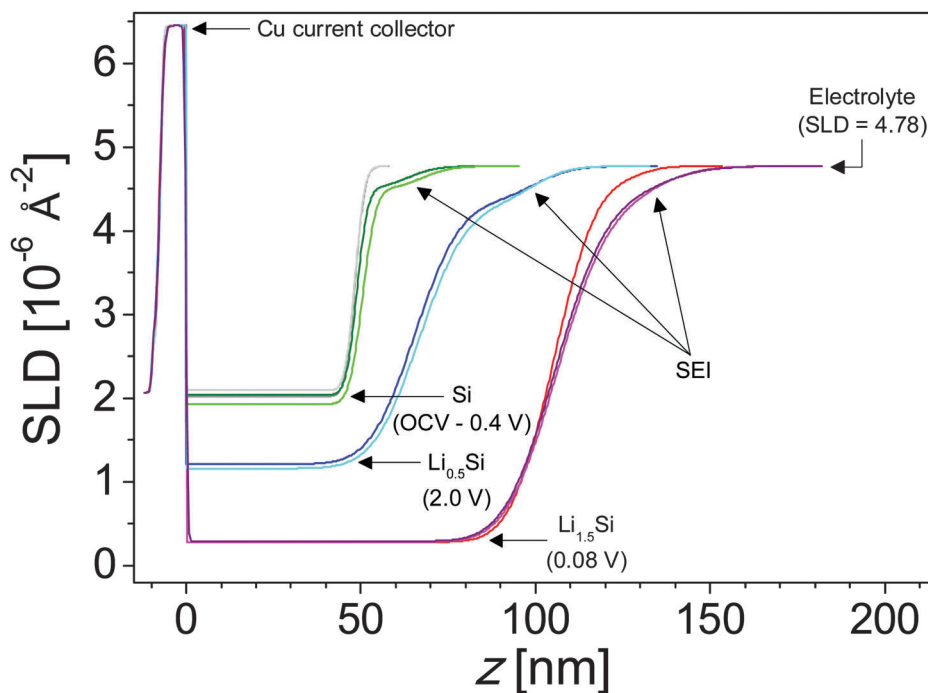
This journal is © the Owner Societies 2016

Fig. 5 SLD profiles representing the tabulated fit parameters (Table 1). Colors match the corresponding fits from Fig. 7. Major layers are labeled.

Table 1 Results of NR fits for electrochemically active components. Additional layers and roughness parameters included in the ESI, Table S1

Potentiostatic voltage	Si Electrode thickness [nm]	Li/Si	SEI thickness [nm]	SEI SLD [10^{-6} Å^{-2}]	$\chi 2$
In air	48.3 ± 0.1				2.2
OCV	48.4 ± 0.1	0.00			2.0
1.1 V	48.3 ± 0.1	0.00			1.8
0.7 V	48.9 ± 0.1	0.01	14.4 ± 3.2	4.5 ± 0.1	2.3
0.4 V	50.5 ± 0.5	0.06	16.7 ± 6.4	4.5 ± 0.2	7.0
0.08 V	106.0 ± 0.3	1.53	26.6 ± 2.1	4.7 ± 0.1	2.9
2.0 V	65.4 ± 1.1	0.45	34.2 ± 7.2	4.3 ± 0.3	4.1
0.08 V	105.9 ± 0.7	1.53	27.3 ± 2.3	4.3 ± 0.1	3.0
2.0 V	66.9 ± 0.6	0.49	32.2 ± 1.5	4.3 ± 0.1	3.2
0.08 V	105.5 ± 0.7	1.52	28.6 ± 4.0	4.3 ± 0.1	3.9

the structure within the NR data consistent with an increased Li–Si ratio and a slight thickening of the SEI layer (14.4 to 16.7 nm), Fig. 5.

Upon further lithiation (0.08 V) we see a significant change in the NR data due to the growth of the Li–Si electrode layer (50.5 to 106 nm) and the further increase in the SEI thickness (16.7 to 26.6 nm). The SLD of the Si-layer decreases from 2.07×10^{-6} Å^{-2} to 0.28×10^{-6} Å^{-2} due to the incorporation of low-SLD Li. Eqn 1 and 2 indicate that lithiation of the electrode results in the alloy $Li_{1.5}Si$, well below the full lithiation capacity of $Li_{3.75}Si$. Furthermore, delithiation of the electrode does not go to completion, resulting in an electrode composition of $Li_{0.45}Si$, suggesting that a significant portion of the Si lithiation capacity is irreversible.

To confirm that the Li/Si ratio determined *via* NR is consistent with the electrochemical results we compared the reversible Li/Si ratio from NR to the reversible electrochemical capacity of the cell.

If the entire electrode area within the O-ring (18 cm^2, 4.8 cm diameter) was lithiated uniformly, the observed reversible electrochemical capacity (142 μA h) indicates that the electrode has a reversible Li capacity of 0.69 Li per Si. This is significantly lower than the changes in electrode thickness from NR (eqn (1)) which suggests that the electrode has a reversible capacity of ∼1.0 Li per Si. Since the Li metal electrode (∼2.9 cm diameter) is smaller than the Si electrode lithiation of the Si appears to occur primarily under the Li counter electrode. A comparison of the Li/Si ratio determined *via* NR and *in situ* charge and discharge capacities suggest an effective Si electrode area of ∼10 cm^2 (3.6 cm diameter), close to the size of the Li counter electrode yet still significantly larger than the NR footprint (4 mm × 2 mm centered on the Si electrode/Li counter electrode). Since the electrode area that contains the NR footprint is centered on the Li counter electrode and much smaller, it is expected to be uniformly lithiated. While a significant portion of the Si electrode does not participate in electrochemical lithiation, Li diffusion from the active area during both electrochemical lithiation and relaxation contributes to lithiation of the inactive area. As long as the Li/Si ratio in the inactive area lies below ∼0.45, Li diffusion will contribute to the irreversible lithiation capacity.

Since the NR cell is not operated under galvanostatic conditions (Fig. 3), it cannot be directly compared to a standard coin cell using differential capacity curves (Fig. 2). Due to the differences in the *iR* drop between the NR and coin cells the recorded voltage for the states of charge was slightly different from that designed in the experiment. However, the compositions and state of charge are close enough to enable comparisons between the NR and the XPS data.

This journal is © the Owner Societies 2016

Phys. Chem. Chem. Phys., 2016, **18**, 13927–13940 | **13933**

As noted previously the SEI thickness increased from 16.7 to 26.6 nm when lithiated to $Li_{1.5}Si$. Interestingly, the SLD of the SEI increased from 4.5 to 4.7×10^{-6} $Å^{-2}$. Since *ex situ* XPS indicates that Li content increases during the first lithiation (Section 3.3), which is expected to decrease SLD, this increase in SLD could be due to a densification of the SEI or an increase in high scattering length nuclei like C, O, F, or ^2H, which is not captured *via* XPS. A large (>66%) increase in SEI porosity (filled with high-SLD electrolyte) could also explain this change; however, we are unaware of any mechanism which would induce such a sudden and significant increase in porosity and further find this explanation unlikely in a period when both *in situ* NR and *ex situ* XPS indicate SEI growth, from 14.4 ± 3.2 nm to 26.6 ± 2.1 nm (NR) and 5.3 ± 2.3 nm to 7.9 ± 3.4 nm (XPS – discussed below).

Upon delithiation the electrode thickness reduces significantly (106 to 65.4 nm) indicating an electrode composition of $Li_{0.45}Si$. Interestingly, the thickness of the SEI increases further to 34.2 nm with a corresponding decrease in the SLD to 4.3 ± 0.3 $\times 10^{-6}$ $Å^{-2}$ indicating an increase in Li content or a decrease in SEI density. Since *ex situ* XPS indicates that Li content is decreasing (Section 3.3) during this stage, the change in SLD is most likely due to a densification (increase in N_d) of the SEI. Upon a second lithiation ($Li_{1.5}Si$) the SEI layer contracts significantly (34.2 to 27.3 nm) while maintaining the SEI SLD. A similar expansion and contraction are observed with additional cycling. This swelling and contracting has been previously observed *via in situ* NR studies on the SEI formed in traditional carbonate electrolytes.[26] The degree of swelling and contraction decreases with additional cycling—a 6.9 nm difference after the first cycle and a 3.6 nm difference after the second cycle—suggesting that the SEI is approaching an equilibrium state. If this contraction and swelling is due in part to changes in the atomic density of the SEI, the lack of corresponding changes in the SLD of the SEI indicates that compositional changes occur in concert with and counteracting the effects of changes in atomic density. The most likely compositional difference is the Li content. Increasing the density of the SEI (contraction) increases the SLD while increasing the Li content reduces the SLD. If the changes in SEI thickness are indicative of changes in atomic density and changes in the SLD are indicative of changes in the Li content of the SEI, the SEI on the Si electrode in the lithiated state ($Li_{1.5}Si$) has both a higher atomic density and higher Li content than the SEI on the Si electrode in the delithiated state ($Li_{0.5}Si$).

3.3 *Ex situ* X-ray photoelectron spectroscopy

Most of the community's understanding of SEI chemistry comes from traditional *ex situ* methods like X-ray photoelectron spectroscopy. To understand how the SEI chemistry determined *via* NR compares with traditional XPS studies a detailed analysis of previously collected XPS data was performed to estimate layer thicknesses and compositions. The published XPS data indicate that the SEI chemistry in the $PF5M_2$ electrolytes is very similar to a standard EC/DMC based electrolyte.[31] Indeed, the SEI was shown to contain LiF and Li_2CO_3 type components as well as

organic carbonates (C 1s: CO_3, 289 eV; O 1s: C=O, 532 eV, and C–O, 533 eV), carboxylates (C 1s: CO_2, 289 eV; O 1s: C=O and C–O), ethers/esters (C 1s: CO, 285.5 eV; O 1s: C–O), and fluorides (C 1s: CF, 287 eV; F1s: CF 689 eV) in similar concentrations. For this work we turned our attention to the Si 2p spectra collected for the samples, which were not previously discussed in great detail. The Si 2p signal intensity can be used to estimate the layer thickness using the following equation:

$$I(A) = F\sigma(A) \sum_i \left(\int_0^{L_i} N_{d,i}(A) e^{-\frac{x}{\lambda_i}} dx \prod_j^{i-1} e^{-\frac{L_j}{\lambda_j}} \right) \quad (3)$$

where $I(A)$ is the (integrated) signal intensity for atom A, F is a prefactor that is determined by the experimental conditions, $\sigma(A)$ is the standard sensitivity factor for atom A, L_i is the thickness of layer i ($i = 1$ for the top layer), λ_i is the electron inelastic mean free path for layer i, and $N_{d,i}(A)$ is the number density (atoms per nm^3) for atom A in layer i. The only source of Si is the electrode and adventitious oxide, so the Si 2p signal (Fig. 6) and eqn (3) can be used to estimate the SEI (layer 1) thickness, since $N_d(Si)$ and the thickness are known for those layers. For the as-fabricated electrodes, no Cu signal from the current collector is detected, so the Si layer (layer 3) can be treated as infinitely thick. Assuming that the adventitious oxide is SiO_2, the oxide layer (layer 2) thickness can be calculated from the ratio of the integrated intensity of the SiO_2 and Si^0 peak in the Si 2p spectrum. In general, λ is material dependent; however, most materials have $\lambda = 3.5 \pm 1.5$ nm.[3,9,37,38] Because there is no simple method for determining λ for arbitrary materials, a uniform $\lambda = 3.5 \pm 1.5$ nm was assumed for all calculations. X-ray attenuation does occur within the sample; however, the penetration depth of X-rays is much larger (~mm assuming insulating samples) than the electron escape depth and can be neglected without the introduction of errors for all subsequent calculations.

For an accurate determination of the SEI thickness, changes in the thickness and $N_d(Si)$ of layers 2 and 3 must be taken into account. Fortunately, the reactions in these layers are relatively
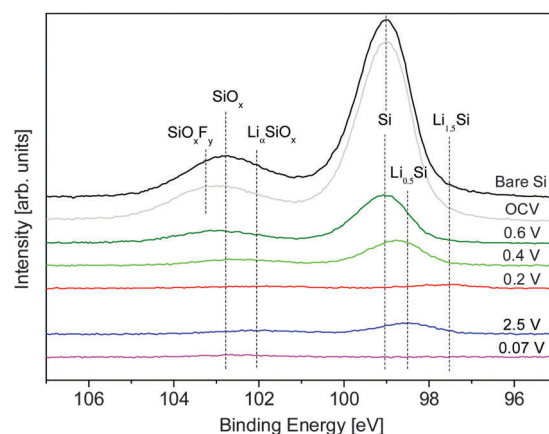

Fig. 6 *Ex situ* Si 2p XPS spectra used to calculate the SEI thickness using eqn (3). Spectra colored to match those of the closest SLD profile determined from NR.

13934 | *Phys. Chem. Chem. Phys.*, 2016, **18**, 13927–13940

This journal is © the Owner Societies 2016

well-defined in the literature and electrochemically well-separated.[3,9,31,39] At 0.5 V, the adventitious oxide (layer 2) undergoes irreversible lithiation ($4e^- + 4Li^+ + SiO_2 \rightarrow 2LiO_2 + Si$) and is assumed to form an intimate mixture of LiO_2 and Si, both of which have well-known densities. At lower voltages (<0.3 V) lithiation of the Si ($xe^- + xLi^+ + Si \rightarrow Li_xSi$) in layers 2 and 3 begins to occur, where $N_d(Si)$ can be determined from eqn (1). Based on the NR results, $x \approx 1.5$ for 0.2 V, $x = 3.75$ for 0.07 V, and $x = 0.5$ for 2.5 V. Although the differential capacity curves indicate that the electrode does not reach full lithiation ($Li_{3.75}Si$) at 0.07 V, assuming full lithiation underestimates SEI thickness and represents the most conservative estimate and is sufficient for analysis. The thickness, composition, and $N_d(Si)$ for each layer as a function of SOC are summarized in Table 2.

Only layer 1 (SEI) contains information that is not defined *a priori* for this analysis so only the properties of that layer can be determined. *Ex situ* XPS shows that the SEI forms electrochemically above 0.6 V (4.5 ± 1.9 nm) followed by continued growth during SiO_2 (0.4 V, 5.3 ± 2.3 nm) and Si (0.2 V, 7.9 ± 3.4) lithiation. A Si signal for the first full lithiation (0.07 V) could not be collected, so it is not possible to determine an SEI thickness for this state; however, given the low reduction stability of the fluorinated electrolyte,[1,31–33] it is likely that the thickness of the SEI in this state is greater than that in the 0.2 V state. The SEI then shrinks during delithiation (2.5 V, 6.9 ± 3.0 nm) and swells during the second lithiation.

To aid in further discussion, the results from the XPS (Table 2) and NR (Table 1) analysis discussed above are summarized graphically in Fig. 8, which compares the thickness and SLD of the SEI as determined *via ex situ* XPS (Fig. 8A and C) and *in situ* NR (Fig. 8B and D). In both cases it can be seen that the SEI layer grows in thickness with lithiation (to 0.2 V) but the magnitude of the increase differs by nearly 10 nm with the SEI layer being thicker when measured *in situ*. This difference in SEI thickness increases to nearly 20 nm after fully lithiating and delithiating the electrode. Furthermore, upon cycling between lithiated and delithiated states we notice a divergent behavior. Specifically, the SEI swelling observed during lithiation measured *via* NR appears to be the opposite for the XPS which shows the SEI layer contracting. Upon lithiation

the NR-measured SEI thickness decreases by ∼6 nm while the XPS-measured thickness increases by ∼4 nm.

We now turn our attention to the compositions estimated from the XPS studies and analysis of the SLD values. After correcting for (attenuated) O and Li signals from the Si and SiO_2 layer, the SLD of the SEI can be estimated directly from the atomic composition determined *via* XPS (excluding hydrogen) (Fig. 7) using eqn (1). Estimating the SLD from the XPS composition requires an assumption of the average atomic density (N_d) of the SEI. For this purpose, a range of model N_d was chosen: high density (LiF), moderate density (Li_2CO_3), and low density (EC). Since the actual N_d of the SEI is unknown changes in the SLD of the SEI will be discussed according to the changes in the atomic composition that most influenced that change. Specifically, changes in C (6.65 fm) and Li (−1.90 fm) content of the SEI will drastically affect the predicted SLD, while changes in F and O ratios (5.65 fm and 5.80 fm, respectively) will not have a significant effect on the SLD of the SEI. H in the form of ^2H (6.67 fm), which is not detected *via* XPS but may be present in the SEI, would tend to increase the SLD. The XPS-derived SLD of the SEI at 0.6 V (22.1 at% Li) is 4.6×10^{-6} Å^{-2} while at 0.4 V (23.8 at% Li) the SLD_{xps} is 4.4×10^{-6} Å^{-2}. These values are similar to the SLDs measured using NR (Fig. 8C and D). After further lithiation the XPS-derived SLD
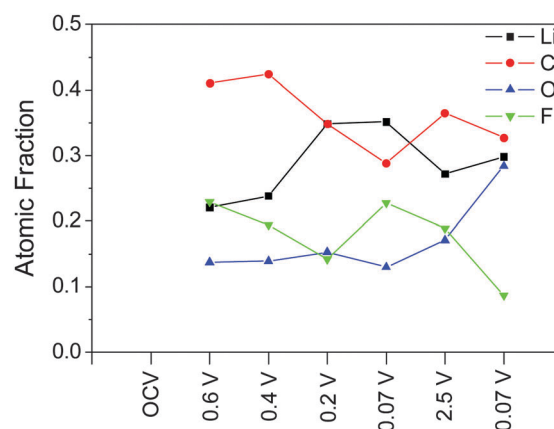

Fig. 7 Atomic compositions of the SEI determined from XPS and used to estimate SLD.

Table 2 Layer thicknesses derived from *ex situ* XPS. Uncertainty derived from $\lambda = 3.5 \pm 1.5$ nm. SLD range of the SEI estimated using the atomic density (N_d) of LiF and EC. High-resolution Si data were not collected for the first 0.07 V sample, due to the fact that no Si signal was detected in the low-resolution spectrum

	Layer 1 (SEI)			Layer 2 (SiO_2)			Layer 3 (Si)	
Potential	Integrated intensity [arb. units]	Thickness [nm]	SLD $N_d = Li_2CO_3$ (EC, LiF) [10^{-6} Å^{-2}]	Composition	Thickness [nm]	N_d (Si) [nm^{-3}]	Composition	N_d (Si) [nm^{-3}]
Bare Si	98.70			SiO_2	1.9 ± 0.8	26.54	Si	49.94
OCV	96.79			SiO_2	1.9 ± 0.8	26.54	Si	49.94
0.6 V	26.40	4.5 ± 1.9	4.6 (4.0, 5.4)	SiO_2	1.9 ± 0.8	26.54	Si	49.94
0.4 V	14.62	5.3 ± 2.3	4.4 (3.9, 5.3)	Li_2O + Si	3.5 ± 1.5	14.43	Si	49.94
0.2 V	3.45	8.0 ± 3.4	3.4 (3.1, 4.1)	Li_2O + $Li_{1.5}Si$	4.6 ± 2.0	10.69	$Li_{1.5}Si$	23.09
0.07 V			3.4 (3.0, 4.0)	Li_2O + $Li_{3.75}Si$				
2.5 V	6.93	6.9 ± 3.0	4.1 (3.6, 4.9)	Li_2O + $Li_{0.5}Si$	3.9 ± 1.7	12.97	$Li_{0.5}Si$	35.99
0.07 V	0.83	12.5 ± 5.4	3.9 (3.4, 4.6)	Li_2O + $Li_{3.75}Si$	5.0 ± 2.2	7.84	$Li_{3.75}Si$	12.78

of the SEI at 0.2 V (34.9 at% Li) is 3.4×10^{-6} Å^{-2} while the SLD of the 0.07 V data (35.2 at% Li) is 3.4×10^{-6} Å^{-2}. These calculated SLDs are significantly lower than what was measured *via* NR, even given the large uncertainty in the electron mean free path. This apparent decrease in the SLD has to be due to extra Li in the washed sample or the removal of C, O, F, and D components during washing, given their large SLDs. Delithiation of the electrode causes the SLD to increase as the Li content drops (2.5 V, 4.1×10^{-6} Å^{-2}, 27.2% Li). The SLD then drops again as the Li content increases during lithiation (0.07 V, 3.9×10^{-6} Å^{-2}, 29.8% Li). These values are much closer to the SLDs determined *via* NR, indicating that the compositions from *ex situ* XPS and *in situ* NR are approaching unity.

The results summarized in Fig. 8 indicate significant differences in the SEI chemistry measured by *ex situ* and *in situ* methods. The differences in composition and thickness are likely correlated and

originate from three potential causes: (1) the lack of hydrogen sensitivity in XPS, (2) differences in porosity caused by drying the SEI prior to *ex situ* analysis, and (3) the removal of SEI components during DMC washing prior to *ex situ* analysis.

It is possible that SLDs calculated from XPS are low due to the insensitivity of XPS to H, which, in the form of ^{2}H (6.67 fm), has a higher scattering length than O (5.80 fm), F (5.65 fm), C (6.65 fm), and Li (−1.90 fm). However, the low hydrogen content of the electrolyte makes this possibility unlikely, and neglecting the hydrogen content fails to explain the observed differences in SEI thickness.

Another possibility is that SEI porosity, which would be present only in the *in situ* cell, is responsible for this discrepancy. Assuming that these pores are filled with the electrolyte, only for the lowest model density $[N_d(\text{SEI}) = N_d(\text{EC})]$ can physically reasonable values of porosity be calculated. Even then, reconciling
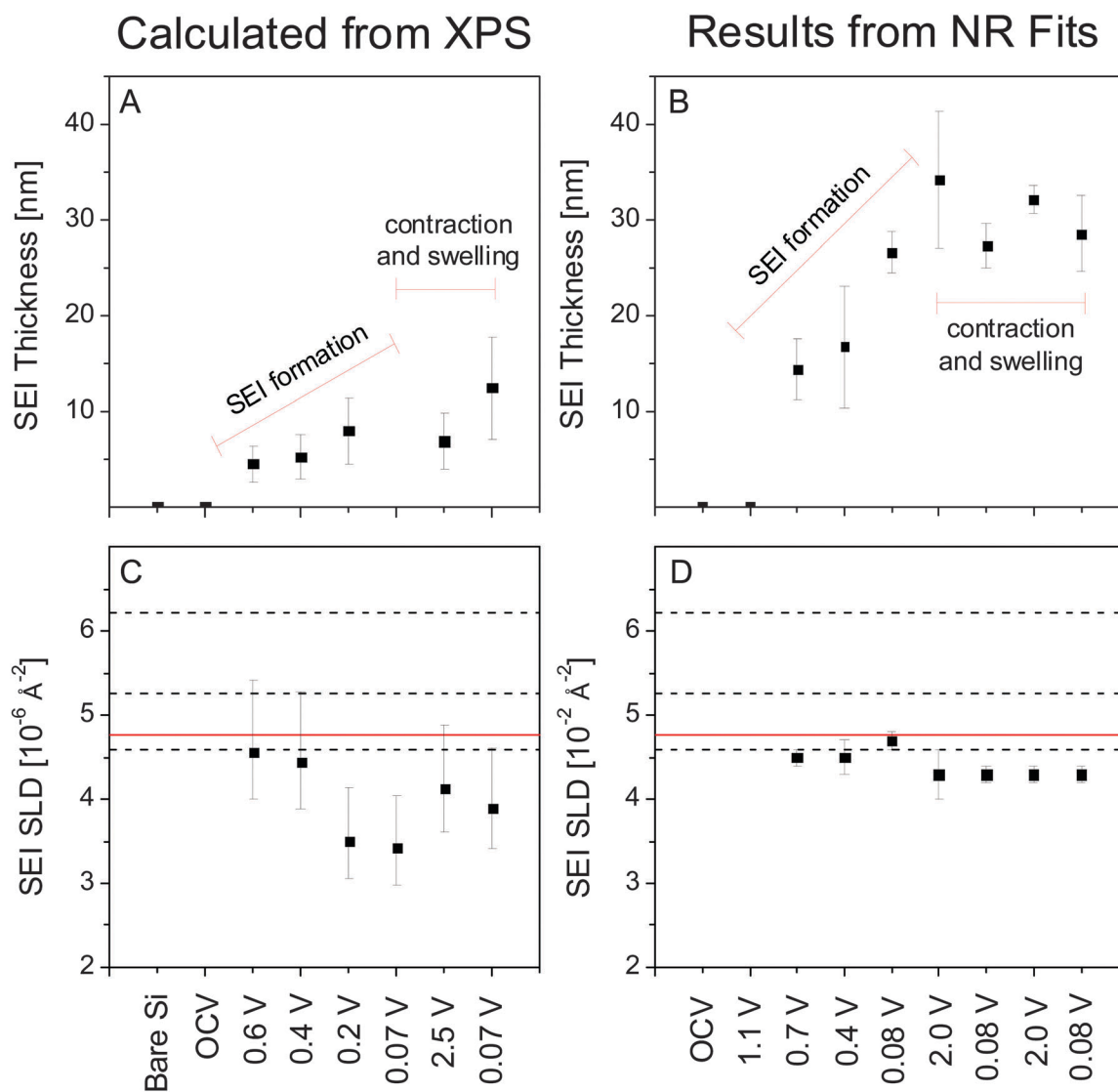

Fig. 8 SEI thickness and SLD as determined *via ex situ* XPS (A and C) and *in situ* NR (B and D). The black dashed lines in C and D indicate the expected SLD for lithium perfluoroglutarate (Section 3.4) at the atomic density of LiF (upper), Li$_2$CO$_3$ (middle), and EC (lower). The solid red line indicates the SLD of the electrolyte.

these values would require 40% to 70% porosity in most of the cases to obtain the SLD observed *via* NR, much higher than what previous studies suggest.[10,40,41] Since this porosity would collapse entirely during drying, prior to collecting XPS data, the thicknesses determined from NR should be 1.7 to 3.3 times as thick as that determined *via* XPS. While this possibility is not explicitly contradicted by the data, it is on the extreme edge of plausibility. For the SEI formed at the end of the first discharge, these values jump to 90–99% porosity and 10 to 100 times swelling. Though a thickness measurement from XPS is not available for this state, it is highly unlikely that an SEI of 0.3 nm to 4.1 nm would be observed. Changes in porosity are also unable to explain why swelling and contracting of the SEI occur during opposite steps when observed through XPS or NR. For these reasons, it is unlikely that porosity of the SEI measured *in situ* is the sole source of the differences between the SEI thickness and the SLD measured *via* XPS or NR.

The third possibility is that rinsing the electrodes prior to XPS, necessary to remove excess electrolyte, dissolves certain components of the SEI. The washing of components from the SEI layer would be consistent with a change in Li/^{2}H content. Specifically, at the initial stages of SEI formation (0.7–0.4 V) a uniform Li-organic layer may have formed which is easy to remove by washing. At 0.2–0.07 V a denser inorganic/organic heterolayer forms. The organic layer can be washed away easily leaving a more inorganic layer comprised of LiF, Li_2CO_3, *etc.* This layer would result in the low SLD predicted from fitting the XPS. The differences in the SEI thicknesses must therefore be due to different ratios of inorganic and removable organic components. At higher voltages there are more organic components forming a thicker layer which are dissolved during washing to leave a thin inorganic layer, explaining the observed XPS and NR data, Fig. 8. Combining *in situ* atomic force microscopy and *ex situ* XPS, Cresce *et al.* have shown that the SEI formed in a carbonate electrolyte (1.32 M LiTFSI in EC) on highly oriented pyrolytic graphite (HOPG) is composed of a hard, primarily inorganic layer on the electrode surface and a soft, organic layer on top of that. Rinsing the HOPG electrode after cycling was shown to remove the soft outer layer of the SEI and leave a layer rich in inorganic carbonates and fluorides.[10] Those results are consistent with the differences observed in this study between *ex situ* XPS and *in situ* NR. The inner, thin Li-rich (low SLD) layer is observed in XPS after washing away the outer, thick organic layer (high SLD) that is observed in NR.

3.4 *Ex situ* nuclear magnetic resonance

We tested explicitly for the formation of species which were soluble in PF5M$_2$, in which most Li salts are not very soluble, and found only minute compositional changes in the electrolyte after cycling. Li salts and organic monomers that are part of the SEI are likely to be much more soluble in DMC, leaving only high molecular weight polymers and highly insoluble Li salts, *e.g.* LiF, Li_2O, and Li_2CO_3, to be detected after washing. NMR was carried out on the electrolyte before and after cycling in order to determine to what extent soluble electrochemical byproducts were formed during cycling. Based on previous observations in this

system using infrared absorption spectroscopy[31] and related electrochemistry accepted in the literature,[1] we contend that the most likely explanation of these minute compositional changes are due to the electrochemical formation of dilithium perfluoroglutarate (PF5Li$_2$) from PF5M$_2$. (Due to the limits of the experiment and ester lability, the presence of lithium methyl perfluoroglutarate (PF5MLi) is assumed, though not explicitly discussed.)

Multinuclear NMR (Fig. 9) of deuterated and protiated electrolytes shows that only subtle changes occur during cycling. Major signals belong to PF5M$_2$ [^{1}H: 1.0 (singlet); ^{13}C: 15.0 (singlet), 109.4 (triplet of triplets), 111.2 (triplet of quintets), 160.2 (multiplet); ^{19}F: −125.2 (singlet), −119.6 (singlet)] and TFSI$^-$ [^{13}C: 120.6 (quartet); ^{19}F: −80.8 (singlet)]. The chemical shift of the CH$_3$ group in the deuterated electrolytes is slightly different from that of the protiated electrolyte (4.00 ppm *vs.* 4.04 ppm in ^{1}H and 54.34 (septet) *vs.* 55.04 ppm (singlet) in ^{13}C). The deuterated electrolytes have a relatively intense peak at 3.85 ppm in the ^{1}H spectrum which is attributed to d$_3$-MeOH formed by hydrolysis of d$_6$-PF5M$_2$ by trace H_2O impurities. The corresponding peak in the protiated electrolytes is obscured by the ^{1}H–^{13}C satellite. The signal for the CH$_3$ of MeOH (^{1}H: 3.6 ppm) appears in the protiated electrolytes but not in the deuterated electrolytes, consistent with the low proportion (<0.6%) of C^{1}H^{2}H$_2$ in the deuterated electrolyte.

Additional signals are of low intensity (<0.1% of primary peaks), illustrating the necessity of using neat (no deuterated solvent) electrolytes during analysis in order to observe impurities and electrochemically formed compounds. All species unique to cycled and uncycled electrolytes appear in both protiated and deuterated electrolytes. The broad peak at 3.7 ppm in the ^{1}H spectrum (Fig. 9A, †) of the cycled, deuterated electrolyte does not show a corresponding intense peak in the protiated electrolyte, suggesting that this peak may be due to an adventitious ^{1}H source, likely ambient H_2O, whose chemical shift is highly environment-dependent.[42,43] Adventitious sources of H have ^{1}H signals that are independent of the level of deuteration of the electrolyte, unlike any hydrogenous species formed from the electrolyte during cycling.

The most significant difference between the cycled and uncycled electrolytes is the intensity and the width of the ^{7}Li signal (Fig. 9B). The changes in peak width for the protiated (3.1 Hz → 13.3 Hz) and deuterated (3.6 Hz → 8.6 Hz) electrolytes with cycling are consistent with the formation of PF5Li$_2$, which would reduce symmetry around the quadrupolar ^{7}Li nuclear, increasing the relaxation rate and the peak width. The intensity of the ^{7}Li signal increases by 18% for the protiated electrolyte and by 28% for the deuterated electrolyte. Though it is difficult to integrate the ^{19}F signals, due to the overlap of intense nearby peaks, the differences in the intensity changes in the ^{7}Li signal are qualitatively consistent with the differences in the intensity of the ^{19}F peaks (Fig. 9D, †) in the protiated and deuterated electrolytes. If due solely to the electrochemical formation of PF5Li$_2$, a 28% increase in the ^{7}Li signal (0.1 M) would correspond to the formation of 14 mM PF5Li$_2$. The appearance of ^{19}F signals (†) with ∼0.003 times the intensity of the primary PF5M$_2$ (5.5 M) peaks at similar chemical shifts is consistent

This journal is © the Owner Societies 2016

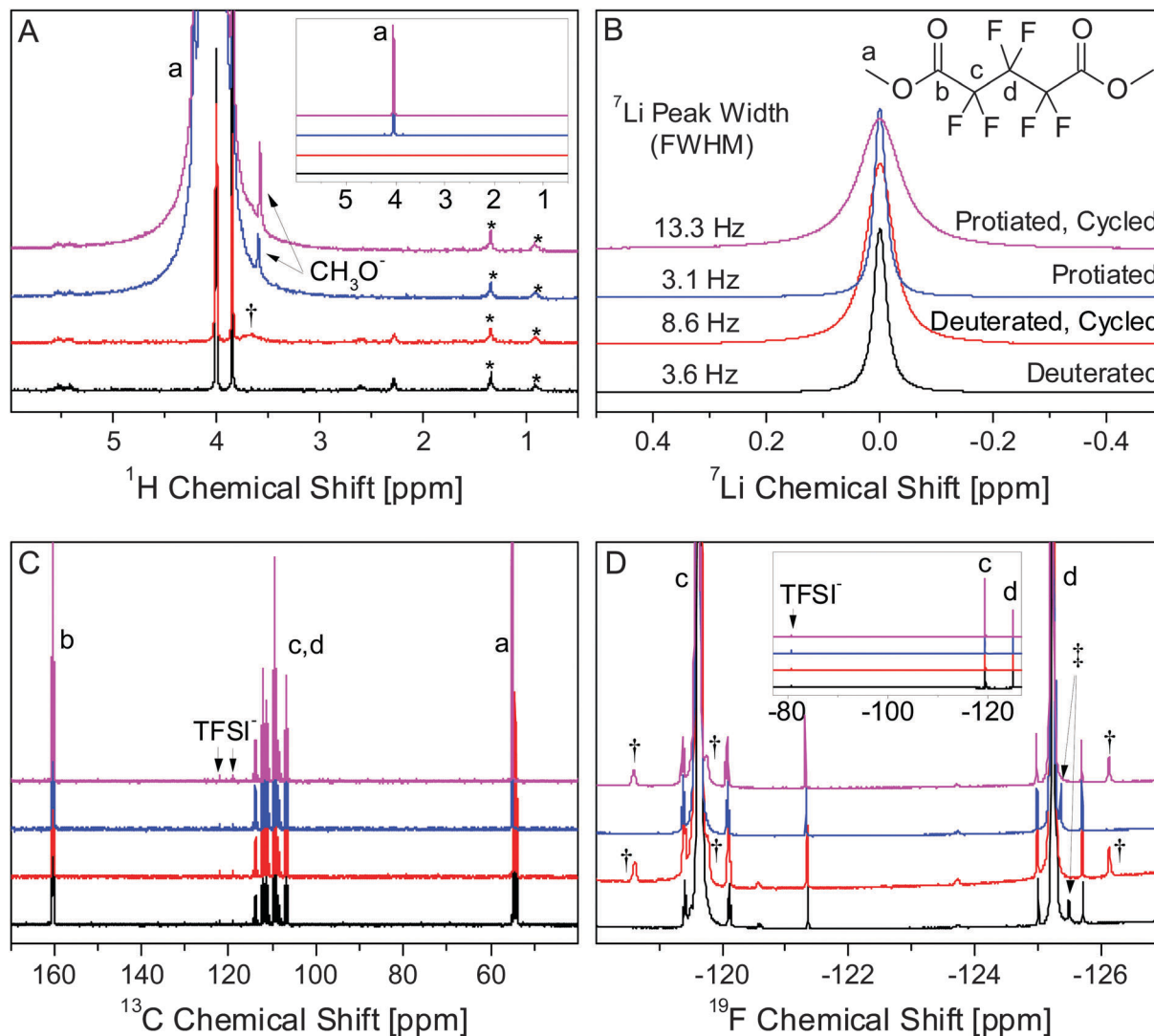*Phys. Chem. Chem. Phys.,* 2016, **18**, 13927–13940 | **13937**

Fig. 9 ^1H (A), ^7Li (B), ^{13}C (C), and ^{19}F (D) NMR spectra of deuterated and protiated electrolytes before and after cycling. Peaks corresponding to PF5M$_2$ (a–d) and the TFSI$^-$ anion are labelled. The insets in ^1H and ^{19}F spectra are 1/1000× scale to show the full intensity of PF5M$_2$ and TFSI$^-$ peaks. Signals unique to the cycled (†) and uncycled (‡) electrolytes as well as signals attributed to volatile species in the epoxy sealant (*) are labelled.

with the formation of PF5Li$_2$. This observation is further evidence that PF5Li$_2$ is the primary soluble product formed during electrochemical cycling. It is, however, unclear whether the differences in the ^7Li spectrum between the protiated and deuterated electrolytes are due to slight differences in the electrochemical discharge conditions, *e.g.* electrolyte volume and cell resistance, or chemical differences caused by an isotopic effect, *e.g.* PF5Li$_2$ solubility.

It is difficult to identify the specific species formed during cycling solely from the chemical shifts in one-dimensional NMR data; though it is clear that only a small number of species (at relatively low concentrations) are formed. Since all other impurity signals present in the uncycled electrolyte except for one (Fig. 9D, ‡) are also present in the cycled electrolyte at roughly the same concentrations, these impurities are most likely electrochemically inert and do not affect SEI formation or composition. Based on the above analysis, PF5Li$_2$ is the only

soluble species formed during electrochemical cycling. Using eqn (2), the SLD of the electrolyte is expected to change from 4.78×10^{-6} Å^{-2} to 4.77×10^{-6} Å^{-2} after discharging the cell. NR is not sensitive to such a small change in the electrolyte SLD, so it is assumed to remain constant during cycling. Additionally, this analysis does not eliminate the possibility of species formed that are soluble in DMC and would be removed during washing prior to *ex situ* XPS.

4. Conclusions

This study provides direct evidence for the contention that rinsing electrodes prior to *ex situ* characterization modifies the SEI, leading to potentially fallacious conclusions about the function, composition, and optimization of SEIs. NR indicates that the PF5M$_2$ electrolyte forms a diffuse SEI that is 32 ± 8 nm thick.

This result is consistent with the generally theorized—albeit broad—range for a typical SEI thickness of one to hundreds of nm[1,10] and similar to previous NR measurements of the thickness of the SEI formed in EC/DMC electrolytes.[26] Both *in situ* NR and *ex situ* XPS indicate that the SEI swells and contracts during cycling. NR indicates that the SEI contracts by up to 22% during lithiation and swells during delithiation, slowly approaching an equilibrium thickness. XPS suggests the opposite, up to 45% contraction during delithiation and swelling during lithiation. XPS also underestimates the SLD of the SEI by up to 25% and underestimates the thickness of the SEI by a factor of 3 to 4. The origin of these differences is the removal of weakly bound surface species on the SEI which is about 20 nm thick.

Acknowledgements

References

1 K. Xu, *Chem. Rev.*, 2014, **114**, 11503–11618.

2 N. Leifer, M. C. Smart, G. K. S. Prakash, L. Gonzalez, L. Sanchez, K. A. Smith, P. Bhalla, C. P. Grey and S. G. Greenbaum, *J. Electrochem. Soc.*, 2011, **158**, A471.

3 B. Philippe, R. Dedryvère, J. Allouche, F. Lindgren, M. Gorgoi, H. Rensmo, D. Gonbeau and K. Edström, *Chem. Mater.*, 2012, **24**, 1107–1115.

4 H. Q. Pham, K. M. Nam, E. H. Hwang, Y. G. Kwon, H. M. Jung and S. W. Song, *J. Electrochem. Soc.*, 2014, **161**, A2002–A2011.

5 P. Verma, P. Maire and P. Novák, *Electrochim. Acta*, 2010, **55**, 6332–6341.

6 K. C. Klavetter, S. M. Wood, Y.-M. Lin, J. L. Snider, N. C. Davy, A. M. Chockla, D. K. Romanovicz, B. A. Korgel, J.-W. Lee, A. Heller and C. B. Mullins, *J. Power Sources*, 2013, **238**, 123–136.

7 C. K. Chan, R. Ruffo, S. S. Hong and Y. Cui, *J. Power Sources*, 2009, **189**, 1132–1140.

8 X. Chen, X. Li, D. Mei, J. Feng, M. Y. Hu, J. Hu, M. Engelhard, J. Zheng, W. Xu, J. Xiao, J. Liu and J.-G. Zhang, *ChemSusChem*, 2014, **7**, 549–554.

9 B. Philippe, R. Dedryvère, M. Gorgoi, H. Rensmo, D. Gonbeau and K. Edström, *Chem. Mater.*, 2013, **25**, 394–404.

10 A. v. Cresce, S. M. Russell, D. R. Baker, K. J. Gaskell and K. Xu, *Nano Lett.*, 2014, **14**, 1405–1412.

11 K. Edström and M. Herranen, *J. Electrochem. Soc.*, 2000, **147**, 3628–3632.

12 O. Dolotko, A. Senyshyn, M. J. Mühlbauer, K. Nikolowski and H. Ehrenberg, *J. Power Sources*, 2014, **255**, 197–203.

13 M. T. McDowell, S. W. Lee, J. T. Harris, B. A. Korgel, C. Wang, W. D. Nix and Y. Cui, *Nano Lett.*, 2013, **13**, 758–764.

14 L. Zhou, M. Leskes, A. J. Ilott, N. M. Trease and C. P. Grey, *J. Magn. Reson.*, 2013, **234**, 44–57.

15 P. Novák, D. Goers, L. Hardwick, M. Holzapfel, W. Scheifele, J. Ufheil and A. Würsig, *J. Power Sources*, 2005, **146**, 15–20.

16 M. Bianchini, E. Suard, L. Croguennec and C. Masquelier, *J. Phys. Chem. C*, 2014, **118**, 25947–25955.

17 I. A. Bobrikov, A. M. Balagurov, C.-W. Hu, C.-H. Lee, T.-Y. Chen, S. Deleg and D. A. Balagurov, *J. Power Sources*, 2014, **258**, 356–364.

18 H. Liu, C. R. Fell, K. An, L. Cai and Y. S. Meng, *J. Power Sources*, 2013, **240**, 772–778.

19 M. Roberts, J. J. Biendicho, S. Hull, P. Beran, T. Gustafsson, G. Svensson and K. Edström, *J. Power Sources*, 2013, **226**, 249–255.

20 X.-L. Wang, K. An, L. Cai, Z. Feng, S. E. Nagler, C. Daniel, K. J. Rhodes, A. D. Stoica, H. D. Skorpenske, C. Liang,

This journal is © the Owner Societies 2016

Phys. Chem. Chem. Phys., 2016, **18**, 13927–13940 | 13939

W. Zhang, J. Kim, Y. Qi and S. J. Harris, *Sci. Rep.*, 2012, **2**, 747.

21 B. Jerliu, L. Dorrer, E. Huger, G. Borchardt, R. Steitz, U. Geckle, V. Oberst, M. Bruns, O. Schneider and H. Schmidt, *Phys. Chem. Chem. Phys.*, 2013, **15**, 7777–7784.

22 J. E. Owejan, J. P. Owejan, S. C. DeCaluwe and J. A. Dura, *Chem. Mater.*, 2012, **24**, 2133–2140.

23 M. Hirayama, N. Sonoyama, T. Abe, M. Minoura, M. Ito, D. Mori, A. Yamada, R. Kanno, T. Terashima, M. Takano, K. Tamura and J. i. Mizuki, *J. Power Sources*, 2007, **168**, 493–500.

24 J. F. Browning, L. Baggetto, K. L. Jungjohann, Y. Wang, W. E. Tenhaeff, J. K. Keum, D. L. Wood and G. M. Veith, *ACS Appl. Mater. Interfaces*, 2014, **6**, 18569–18576.

25 G. M. Veith, L. Baggetto, R. L. Sacci, R. R. Unocic, W. E. Tenhaeff and J. F. Browning, *Chem. Commun.*, 2014, **50**, 3081–3084.

26 G. M. Veith, M. Doucet, J. K. Baldwin, R. L. Sacci, T. M. Fears, Y. Wang and J. F. Browning, *J. Phys. Chem. C*, 2015, **119**, 20339–20349.

27 A. Nelson, *J. Appl. Cryst.*, 2006, **39**, 273–276.

28 T. Heitmann and W. Montfrooij, *Practical Neutron Scattering at a Steady State Source*, Mizzou Media – University BookStores, 2012.

29 M. Wagemaker, R. van de Krol and A. A. van Well, *Physica B: Cond. Mat.*, 2003, **336**, 124–129.

30 M. Hirayama, M. Yonemura, K. Suzuki, N. Torikai, H. Smith, E. Watkinsand, J. Majewski and R. Kanno, *Denki Kagaku*, 2010, **78**, 413–415.

31 T. M. Fears, R. L. Sacci, J. G. Winiarz, H. Kaiser, H. Taub and G. M. Veith, *J. Power Sources*, 2015, **299**, 434–442.

32 L. Hu, Z. Xue, K. Amine and Z. Zhang, *J. Electrochem. Soc.*, 2014, **161**, A1777–A1781.

33 Z. Zhang, L. Hu, H. Wu, W. Weng, M. Koh, P. C. Redfern, L. A. Curtiss and K. Amine, *Energy & Environmental Science*, 2013, **6**, 1806.

34 T. Böttcher, B. Duda, N. Kalinovich, O. Kazakova, M. Ponomarenko, K. Vlasov, M. Winter and G. V. Röschenthaler, *Prog. Solid State Chem.*, 2014, **42**, 202–217.

35 O. Arnold, J. C. Bilheux, J. M. Borreguero, A. Buts, S. I. Campbell, L. Chapon, M. Doucet, N. Draper, R. Ferraz Leal, M. A. Gigg, V. E. Lynch, A. Markvardsen, D. J. Mikkelson, R. L. Mikkelson, R. Miller, K. Palmen, P. Parker, G. Passos, T. G. Perring, P. F. Peterson, S. Ren, M. A. Reuter, A. T. Savici, J. W. Taylor, R. J. Taylor, R. Tolchenov, W. Zhou and J. Zikovsky, *Nuclear Instruments and Methods in Physics Research Section A: Accelerators, Spectrometers, Detectors and Associated Equipment*, 2014, **764**, 156–166.

36 V. L. Chevrier and J. R. Dahn, *J. Electrochem. Soc.*, 2009, **156**, A454–A458.

37 S. Tanuma, C. J. Powell and D. R. Penn, *Surf. Interface Anal.*, 2005, **37**, 1–14.

38 S. Tanuma, C. J. Powell and D. R. Penn, *Surf. Interface Anal.*, 2011, **43**, 689–713.

39 P. R. Abel, Y.-M. Lin, H. Celio, A. Heller and C. B. Mullins, *ACS Nano*, 2012, **6**, 2506–2516.

40 P. Lu and S. J. Harris, *Electrochem. Commun.*, 2011, **13**, 1035–1037.

41 S. Shi, P. Lu, Z. Liu, Y. Qi, L. G. Hector, H. Li and S. J. Harris, *J. Am. Chem. Soc.*, 2012, **134**, 15476–15487.

42 H. E. Gottlieb, V. Kotlyar and A. Nudelman, *J. Org. Chem.*, 1997, **62**, 7512–7515.

43 G. R. Fulmer, A. J. M. Miller, N. H. Sherden, H. E. Gottlieb, A. Nudelman, B. M. Stoltz, J. E. Bercaw and K. I. Goldberg, *Organometallics*, 2010, **29**, 2176–2179.

13940 | *Phys. Chem. Chem. Phys.*, 2016, **18**, 13927–13940

This journal is © the Owner Societies 2016